Effect of the Stark shift on the low-energy interference structure in strong-field ionization

Weifeng Yang,[1,2,3,*] Jie Li,[1] Wenbin Jia,[1] Hongdan Zhang,[1,2] Xiwang Liu,[1,2] Ming Zhu,[1] Xiaohong Song,[1,2,3] and Jing Chen[4,5,†]

[1]*Research Center for Advanced Optics and Photoelectronics, Department of Physics, College of Science, Shantou University, Shantou, Guangdong 515063, China*

[2]*Institute of Mathematics, Shantou University, Shantou, Guangdong 515063, China*

[3]*MOE Key Laboratory of Intelligent Manufacturing Technology, Shantou University, Shantou, Guangdong 515063, China*

[4]*HEDPS, Center for Applied Physics and Technology, Peking University, Beijing 100084, China*

[5]*Institute of Applied Physics and Computational Mathematics, P.O. Box 8009, Beijing 100088, China*

(Received 17 September 2020; revised 30 March 2021; accepted 19 April 2021; published 7 May 2021)

An improved quantum trajectory Monte Carlo method including the Stark shift of the initial state, Coulomb potential, and multielectron polarization-induced dipole potential is adopted to revisit the origin of the low-energy interference structure in the photoelectron momentum distribution of the xenon atom subjected to an intense laser field, and resolve the different contributions of these three effects. We found that the Stark shift plays an essential role on the low-energy interference structure, which moves the ringlike constructive interference structure to the lower momentum region. The formation of the low-energy interference structure is a result of the combined effects of Stark shift, laser, and Coulomb fields, while the multielectron polarization mainly enhance the probability of the low energy photoelectron spectrum. Our finding provides insight into the electron dynamics of atoms and molecules when driven by the intense laser fields.

DOI: 10.1103/PhysRevA.103.053105

I. INTRODUCTION

Photoionization of atoms and molecules under intense laser irradiation is a fundamental process in light–matter interaction [1–6]. Because of its very high intensity, which is comparable to the potential fields, the laser field dominates the motion of the electrons released from the atoms and molecules. Therefore, some important issues in strong-field physics, such as above-threshold ionization (ATI), high-harmonic generation, etc., were described using the strong-field approximation (SFA) [7–12] in which the ion potential effect on the emitted photoelectron in continuum was ignored. However, numerous experimental and theoretical evidences have pointed out the faultiness due to the neglect of the Coulomb potential effect. For example, the low-energy structure (LES), i.e., a series of low-energy peaks along the laser polarization direction, has been observed in the photoelectron spectra of atoms subjected to an intense infrared laser field [13–16]. The LES was absent in the SFA simulation, while it was predicted by the numerical solution of the time-dependent Schrödinger equation (TDSE) [13]. Theoretical studies based on Coulomb-corrected SFA theories have demonstrated that the LES is related to the long-range Coulomb potential effect [14,15,17–20].

Subsequently, a radial interference structure in the low-energy region of the photoelectron momentum distribution (PEMD), i.e., the so-called low-energy interference structure (LEIS), has been widely observed in photoionization of different atoms (He, Ne, Ar, Kr, and Xe) [21–23], but the origin of the structure remains obscure and debated [22–26]. The Coulomb potential effect on the classical angular momentum distribution and the minimum number of absorbed photons needed to reach the threshold in multiphoton ionization were discussed with a classical trajectory Monte Carlo method [25,26]. Recently, the PEMD for a hydrogen atom ionized by an intense laser field was investigated using a semiclassical two-step model (SCTS) [27], which found that the LEIS is related to the Coulomb potential effect [28].

Besides the effects of the Coulomb potential, the imprints of multielectron polarization effect have been found in photoelectron spectra [27,29–38]. With a method based on tunnel ionization in parabolic coordinates with inclusion of the Coulomb potential, the polarization induced dipole and the Stark shift of the initial state, Shvetsov-Shilovski *et al.* found that the multielectron polarization affects both the tunneling exit point and the subsequent dynamics, which thus determine the PEMD in elliptically polarized pulses [30]. Further investigation revealed that the multielectron polarization effect increases the distance from the parent ion to the tunnel exit point of the photoelectron and weakens the interaction between them, so that the photoelectron angular distributions are different for different atomic species [39]. Recently, it was shown that the relative yields of the LES are enhanced owing to the multielectron polarization potential on the recolliding electrons [34]. Moreover, it was found that the electron focusing by the multielectron polarization-induced dipole potential (MEPIDP) can induce narrowing of the longitudinal momentum distributions of photoelectrons ionized by a linearly polarized laser pulse [27].

*wfyang@stu.edu.cn
†chen_jing@iapcm.ac.cn

In contrast to the effects of Coulomb potential and MEPIDP, the Stark shift of the initial state has rarely been noticed, partly because it is usually accompanied by the effect of MEPIDP. The Stark shift effect in the strong-field ionization of oriented polar molecules by circularly polarized laser pulses has been investigated using a Stark-shift corrected strong-field approximation (SSFA) method [36]. In comparison with polar molecules, the Stark shift effect in the ionization of atoms has usually been overlooked. Especially, to the best of our knowledge, the contribution of the Stark shift effect to the interference of the electron wave packet (EWP) is still unclear.

In this work we revisit the LEIS in the PEMD of the xenon atom, which is a typical multielectron system, by using an improved quantum trajectory Monte Carlo (IQTMC) method that includes the Stark shift of the initial state, the Coulomb potential, and the MEPIDP. By comparing with the TDSE and SFA results, we resolve the different effects of these three phenomena on the LEIS, and identify that MEPIDP can indeed enhance the yield of the LEIS, but the detailed pattern of the interference fringes depends sensitively on the Coulomb potential and Stark shift. We find that the Stark shift can substantially affect the phase distributions of the EWP. The semiclassical simulation can reproduce the TDSE result well only when the Stark shift is included.

This paper is organized as follows. In Sec. II we briefly discuss the IQTMC method that includes the Stark shift of the initial state, Coulomb potential, and MEPIDP. In Sec. III we show the different characteristics of the fringes of the LEIS in PEMDs obtained with different laser intensities. Second, the underlying mechanism of the LEIS is discussed based on the semiclassical statistical back-trajectory based analysis. The conclusions are presented in Sec. IV.

II. IMPROVED QUANTUM TRAJECTORY MONTE CARLO METHOD

In this work we adopt the IQTMC method. This method combines the Ammosov-Delone-Krainov (ADK) theory with Feynman's path integral approach. Briefly, the initial conditions of all the involved electrons are simulated by the ADK theory, and the phase of each trajectory is included with the classical action after tunneling based on Feynmain's path integral approach so as to describe the quantum interference effects [27,34,40–44]. The motion of the tunnel-ionized electron is determined by the classical Newtonian equation (atomic units are used throughout unless stated otherwise):

$$\frac{d^2\vec{r}}{dt^2} = -\vec{F}(t) - \nabla V_{\mathrm{TOT}}(\vec{r}, t), \tag{1}$$

where $\vec{F}(t)$ is the electric field of the laser pulse. We consider a linearly polarized laser field $\vec{F}(t) = \vec{F}_0 f(t)\cos\omega t$ with peak electric field F_0 and laser frequency ω. The envelope function $f(t)$ is as follows:

$$f(t) = \begin{cases} \cos^2\frac{(t-2T)\pi}{4T}, & 0 < t \leqslant 2T, \\ 1, & 2T < t \leqslant 6T, \\ \cos^2\frac{(t-6T)\pi}{4T}, & 6T < t \leqslant 8T, \\ 0, & t > 8T, \end{cases} \tag{2}$$

where T is the laser optical period. To be more realistic, the envelope should have turning on and turning off parts. The total ionic potential V_{TOT}, including the Coulomb and ionic core polarization potential, is expressed as (the detailed derivation can be seen in Ref. [36])

$$V_{\mathrm{TOT}}(\vec{r}, t) = V_{\mathrm{CP}}(\vec{r}, t) + V_{\mathrm{IDP}}(\vec{r}, t), \tag{3}$$

where $V_{\mathrm{CP}}(\vec{r}) = -Z/|\vec{r}|$ is the hydrogenlike Coulomb potential, and $Z = \sqrt{2I_p}$ is the effective nuclear charge. The second term denotes MEPIDP, i.e., the ionic core polarization induced by the laser field [45], which has the following form:

$$V_{\mathrm{IDP}}(\vec{r}, t) = -\alpha_I \vec{F}(t)\cdot\vec{r}/r^3, \tag{4}$$

where α_I is the static polarizability of the single charged ion. Because the MEPIDP is divergent at the origin, a cutoff point r_c is introduced where the core polarization cancels the laser field, with $\alpha_I E(t)/r_c^2 - r_c E(t) = 0$, which results in $r_c = \alpha_I^{1/3}$ [34,38]. When $r \leqslant r_c$, the electron is nearly field free and will not experience polarization effects.

In order to solve Eq. (1), we need to obtain the initial position and velocity of the electron. The initial position, i.e., the tunnel exit point can be determined by the Schrödinger equation in a uniform field F in a parabolic coordinate [30] as follows:

$$\frac{d^2 f(\eta)}{d\eta^2} + 2\left(-\frac{1}{4}I_p(F) - V(\eta, F)\right) f(\eta) = 0, \tag{5}$$

where the effective potential is expressed as

$$V(\eta, F) = -\frac{1 - \sqrt{2I_p(F)}/2}{2\eta} - \frac{1}{8}\eta F - \frac{1}{8\eta^2} + \frac{\alpha_I F}{\eta^2}. \tag{6}$$

Physically, Eq. (5) describes a tunneling process for an electron with energy of $-\frac{1}{4}I_p(F)$ within an effective potential of $V(\eta, F)$. Therefore, the tunnel exit point η_e can be determined by solving the equation $V(\eta, F) = -\frac{1}{4}I_p(F)$. In Cartesian coordinates, the tunnel exit point is $z_e \approx -\eta_e/2$, i.e.,

$$z_e \approx -\frac{I_p(F) + \sqrt{I_p^2(F) - 4\beta_2(F)F}}{2F}, \tag{7}$$

where

$$\beta_2(F) = Z - (1 + |m|)\sqrt{2I_p(F)}/2, \tag{8}$$

where m is the magnetic quantum number.

The Stark shift is included in the IQTMC model by considering the laser field dependent ionization potential [46]

$$I_p(F) = I_p(0) + \tfrac{1}{2}(\alpha_N - \alpha_I)F^2, \tag{9}$$

where $I_p(0)$ is the field-free ionization potential, α_N is the static polarizability of an atom, and F is the instantaneous laser field at the tunneling ionization instant of the electron. The field-induced term of Eq. (9) should not exceed 10%–20% of the first term, which introduces an upper bound for the magnitude of the laser intensity [27].

We assume that the electron starts with zero initial velocity along the direction of the laser field and nonzero initial velocity $v_\perp$ in the perpendicular direction. The ionization rate at the tunnel exit point is given by the Ammosov-Delone-Krainov

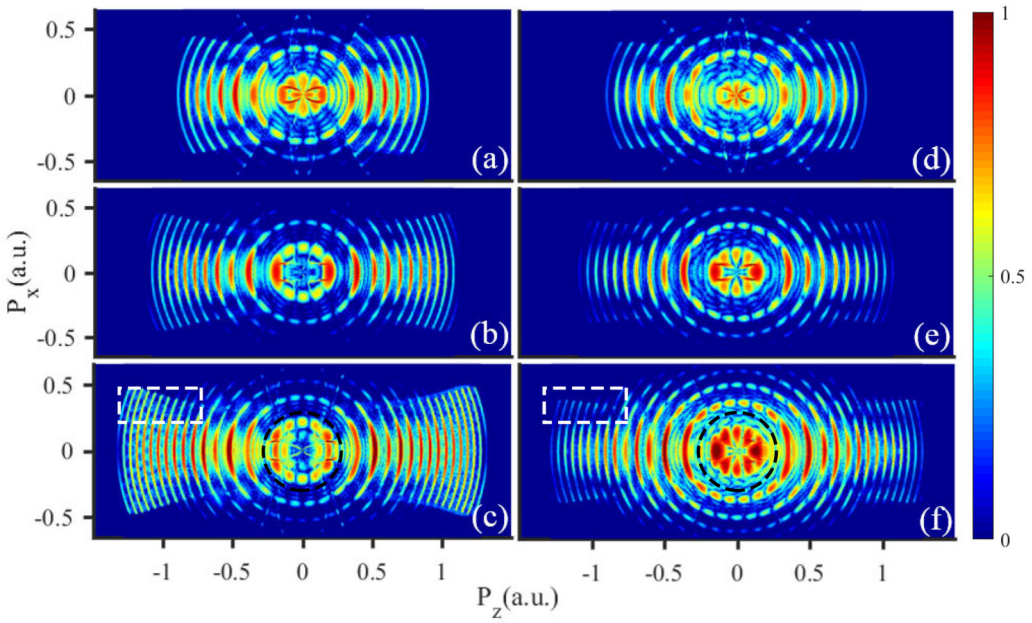

FIG. 1. Simulated two-dimensional (2D) photoelectron momentum spectra of a Xe atom ionized by a laser pulse with a duration of $n = 8$ cycles, at a wavelength of 800 nm. (a) and (d) $I = 1.05 \times 10^{14}$ W/cm^2 corresponding to the Keldysh parameter $\gamma = 0.9829$, (b) and (e) $I = 1.5 \times 10^{14}$ W/cm^2, $\gamma = 0.8223$, and (c) and (f) $I = 2.0 \times 10^{14}$ W/cm^2, $\gamma = 0.712$. The left column [(a)–(c)]: QTMC calculations considering only the Coulomb potential. The right column [(d)–(f)]: IQTMC calculations considering the Coulomb potential, Stark shift, and MEPIDP.

formula [47,48]

$$\Gamma(t_0, v_\perp) = \exp\left(-\frac{2[2I_p(F)]^{3/2}}{3F}\right)\exp\left(-\frac{v_\perp^2\sqrt{2I_p(F)}}{F}\right) \tag{10}$$

Therefore, the intensity must not be very low so that the Keldysh parameter $\gamma = \omega Z/F$ is less than or approximately equal to one. Based on the strong-field Feynman's path integral approach [49,50], the phase of the electron trajectory is expressed as

$$\phi_j(\vec{p}, t_0) = I_p(F)t_0 - \int_{t_0}^{+\infty}\left\{\vec{v}_{\vec{p}}^{\,2}(\tau)/2 + V_{\mathrm{TOT}}(\vec{r}, t)\right\}d\tau, \tag{11}$$

where $\vec{p}$ is the asymptotic momentum of the jth electron trajectory. The probability of each asymptotic momentum is determined as

$$|\Psi_{\vec{p}}|^2 = \left|\sum_j \sqrt{\Gamma(t_0, v_\perp^j)}\exp(-i\phi_j)\right|^2. \tag{12}$$

For the Xe atom, we use the polarizabilities of the statistical theoretical values $\alpha_{\mathrm{Xe}}^N = 25.5$ a.u., $\alpha_{\mathrm{Xe}}^I = 20$ a.u. [51].

III. RESULTS AND DISCUSSION

Figure 1 shows the PEMDs of the Xe atom driven by 800 nm linearly polarized laser fields of different peak intensities $I = 1.05 \times 10^{14}$ W/cm^2 [$\gamma = 0.98$, see Figs. 1(a) and 1(d)], $I = 1.5 \times 10^{14}$ W/cm^2 [$\gamma = 0.82$, see Figs. 1(b) and 1(e)], and $I = 2.0 \times 10^{14}$ W/cm^2 [$\gamma = 0.71$, see Figs. 1(c) and 1(f)]. To resolve the effects of the Coulomb potential, Stark shift, and MEPIDP, we compare the PEMDs calculated by the IQTMC method, which considers all the three effects [Figs. 1(d)–1(f)], with those by the QTMC method, which considers only the effect of the Coulomb potential [Figs. 1(a)–1(c)]. We find that the Stark shift and MEPIDP have obvious influences on the PEMDs, especially on the LEIS. For a low-intensity driven laser field, the LEIS shows radial fanlike fringes for both IQTMC and QTMC simulations [28]. However, the fanlike fringes are shorter in the IQTMC simulation than in the QTMC results [see Figs. 1(a) and 1(d)]. When the laser intensity is increased, the fringes become longer and stronger in the PEMDS of the IQTMC simulations [see Figs. 1(e) and 1(f)]. In contrast, the radial fanlike fringes are split by a ringlike destructive interference structure in the PEMDS of the QTMC simulations [see Figs. 1(b) and 1(c)]. In the high energy region, the longitudinal fringes in the PEMD are weaker when considering MEPIDP and Stark shift than those without considering these two effects [see the white rectangular region in Figs. 1(c) and 1(f)]. And the narrowing effect of the longitudinal PEMDs can be observed, which is consistent with that observed in Mg and Ca [27]. In the following we mainly focus on the low-energy region of the PEMDs ($P_r \in [-0.27, 0.27]$ a.u.).

We first perform the 3D-TDSE simulation in the single-active electron approximation (SAE) by using the finite difference time domain method [52–55]. An atomic model potential of inert gas Xe is adopted in the TDSE simulation [56]

$$V(r) = -\frac{1 + a_1 e^{-a_2 r} + a_3 r e^{-a_4 r} + a_5 e^{-a_6 r}}{r}, \tag{13}$$

where a_i's are gotten from Ref. [56] which are obtained by fitting the numerical potential calculated from the self-interaction free density functional theory. The model potential

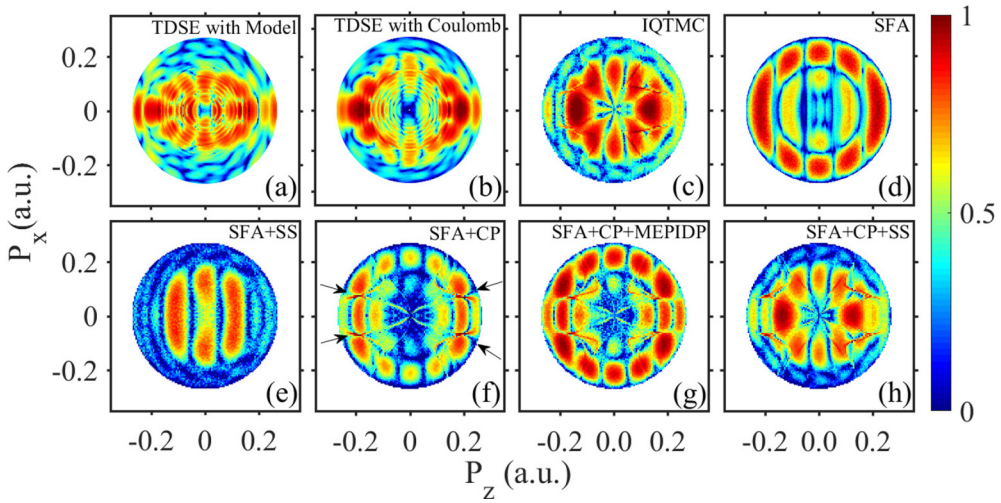

FIG. 2. LEIS ($P_r \in [0, 0.27]$ a.u.) in the photoelectron momentum spectra. (a) and (b) TDSE simulations with model potential (a) and Coulomb potential (b), respectively. (c) Results of the IQTMC calculations (d)–(h) semiclassical simulations with (d) SAF simulation; (e) only laser field and Stark shift are included; (f) only laser field and Coulomb potential are included; (g) with inclusion of laser field, Coulomb potential, and MEPIDP; and (h) with inclusion of laser field, Coulomb potential, and Stark shift. The color scales have been normalized for comparison. The laser parameters are the same as those in Figs. 1(c) and 1(f).

considers the Coulomb potential and shielding of multielectron more accurately than the hydrogenlike potential.

Figures 2(a) and 2(b) show the comparison of the two TDSE simulation results with model potential [Fig. 2(a)] and Coulomb potential [Fig. 2(b)]. The laser parameters are the same as those used in Fig. 1(f). One thing should be noted that the Stark shift is inherent, whereas the multielectron polarization effect is absent in the TDSE simulations for both potentials. However, the multielectron polarization effect is absent in both cases. It can be seen that the main difference between the two simulation results lies in the yield of LEIS. The probability of the fanlike fringes in the low-energy region is higher and the fringes are shorter for simulation with model potential, demonstrating a stronger focusing effect.

Figure 2(c) shows the IQTMC simulation result obtained by considering all the Coulomb potential, the Stark shift, and the multielectron polarization, which reproduces well the main feature of the 3D TDSE simulations. Comparing with TDSE, the semiclassical IQTMC method is more transparent which allows us to disentangle the different contributions of these three effects. For that we first present the result of SFA in Fig. 2(d), where only the laser field is present, and then we compare it with the cases with the three factors included separately or jointly. Obviously the SFA simulation result is significantly different from both TDSE and IQTMC results: (i) vertical interference structure along P_x can be seen which has been known induced by a temporal double-slit interference [57,58]; and (ii) an ATI ringlike interference minimum separate the vertical interference structure. When only the Stark shift is included in the SFA method, see Fig. 2(e), the ring-shaped constructive interference in SFA simulation moves to lower energy part, whereas when only the Coulomb potential is included, see Fig. 2(f), the positions of the ATI rings do not change, which is consistent with the conclusion in Ref. [59]. However, the Coulomb potential makes the vertical temporal double-slit interference slightly along the radial direction, moreover, it induces more interference nodal lines (indicated by the arrows). We analyzed the trajectories contributed to the Coulomb potential induced interference minimum, and found that these interference minima are induced by the interference between the direct and rescattering electron trajectories, i.e., the photoelectron holographiclike interference.

When the MEPIDP is further included [see Fig. 2(g)], the interference pattern has little change except for a higher probability [27]. On the contrary, when the Stark shift is added in place of the mulielectron polarization effect [see Fig. 2(h)], the ringlike constructive interference fringe shrinks to low-energy region. And the radial fanlike fringes can now be clearly seen. On this basis, if the MEPIDP is further included, i.e., the full IQTMC simulation [see Fig. 2(c)], the probability of these LEIS would be enhanced while keep the fringe shapes unchanged. All these results demonstrate that the shapes of the LEIS is determined mainly by the Stark shift and the Coulomb potential, while the multielectron polarization mainly affects the probability of LEIS.

Next we focus on analyzing how the Stark shift influences the momentum spectrum. Because the ionization driven by the linearly polarized laser field has an intrinsic cylindrical symmetry. In our case, the laser is polarized along z axis, so the positive P_x half-plane is exactly the same as the negative P_x half-plane. For convenience, in the following, we analyze the positive half-plane $P_x \geqslant 0$ a.u. Figures 3(b) and 3(c) show the half-plane momentum spectrum with (b) and without (c) Stark shift. To investigate the effect of Stark shift on the phases of trajectories, we extracted trajectories contributing to the central slice of momentum spectrum denoted by magenta rectangular frames and analyze the phases of these contributing trajectories (here we only show the direct ionization electron). Each color denotes that electrons come from different ionization times shown in Fig. 3(a). It can be found that LEIS is indeed related to the phases of trajectories

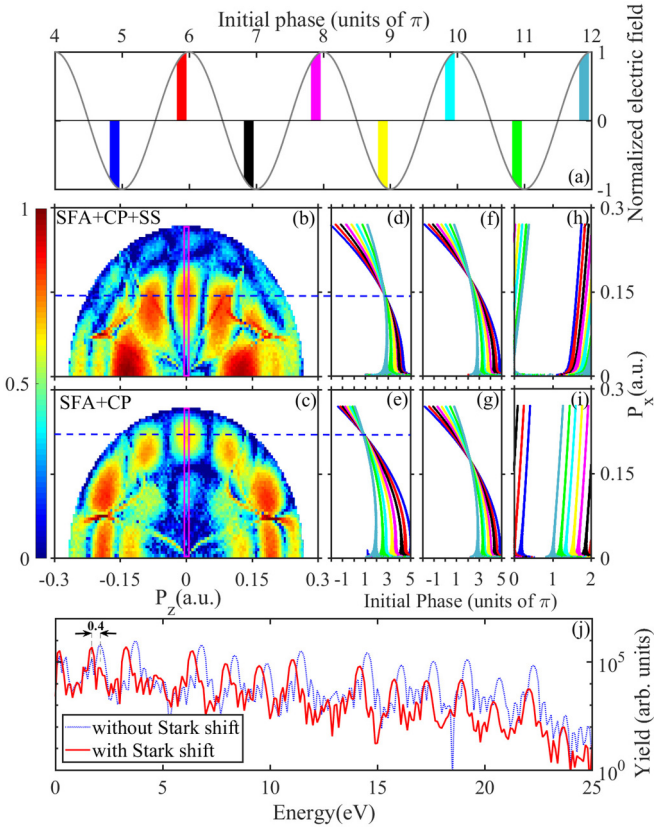

FIG. 3. (a) Subcycle time windows in which photoelectrons contributing to the momentum distributions ($P_x \geqslant 0$ a.u.) of the low-energy part. (b) and (c) The half-plane momentum spectrum with (b) and without (c) Stark shift. ($P_x \geqslant 0$ a.u.) (d) and (e) Final phase distributions of the electron trajectories emitted from different time windows denoted by the same color in (a). (f) and (g) The phase calculated by the integral terms, i.e., the second term in Eqs. (11) and (14), respectively. (h) and (i) Initial phase related to ionization potential, i.e., the first term in Eqs. (11) and (14), respectively. (j) Energy spectrum of photoelectron with (red solid line) and without (blue dotted line) considering the Stark shift.

ionized from different half-cycles of the laser field which depend sensitively on the Stark shift. When the Stark shift is included, the momentum position of constructive interference moves to lower momentum [see Figs. 3(d) and 3(e)], which is consistent with the momentum spectra.

The phase of the electron trajectory in the IQTMC is calculated according to Eq. (11) with Stark shift described by Eq. (9). When the Stark shift is removed, the phase of the electron trajectory would be

$$\phi_j(\vec{p}, t_0) = I_p(0)t_0 - \int_{t_0}^{+\infty} \left\{\vec{v}_{\vec{p}}^{\,2}(\tau)/2 + V_{\mathrm{TOT}}(\vec{r}, t)\right\} d\tau. \quad (14)$$

Figures 3(f) and 3(h) and Figs. 3(g) and 3(i) show the phase contributions of the two terms in Eqs. (11) and (14), respectively. The integral terms in Eqs. (11) and (14) are the same [see Figs. 3(f) and 3(g)]. The main difference lies in the first term. The laser field dependent term $\frac{1}{2}(\alpha_N - \alpha_I)F^2$ not only shifts the final phase but also make the variation of phases between different cycles significantly smaller [see Figs. 3(h) and 3(i)], which results in that the momentum position where the total phases of trajectories ionized from different half-cycles are the same moves to lower P_x, see Figs. 3(d) and 3(e). This explains well the phenomenon that the constructive interference in the final PEMD moves to the low momentum region and makes the LEIS change from a ringlike to fanlike pattern after considering Stark shift. The momentum shift is exactly quantitatively consistent with the energy shift in energy spectrum, see Fig. 3(j), which is obtained by integrating over all photoelectron with the same energy. We further quantify this energy shift from the above laser field dependent term $\frac{1}{2}(\alpha_N - \alpha_I)F^2$. As we know, the probability of ionization is greatest near the peak of the electric field. Thus, we might as well make F equal the peak value of the electric field to quantify the variation amplitude which equals 0.4209 eV, and the shift in energy spectra is 0.4 eV, being consistent with the ionization potential shift quantitatively.

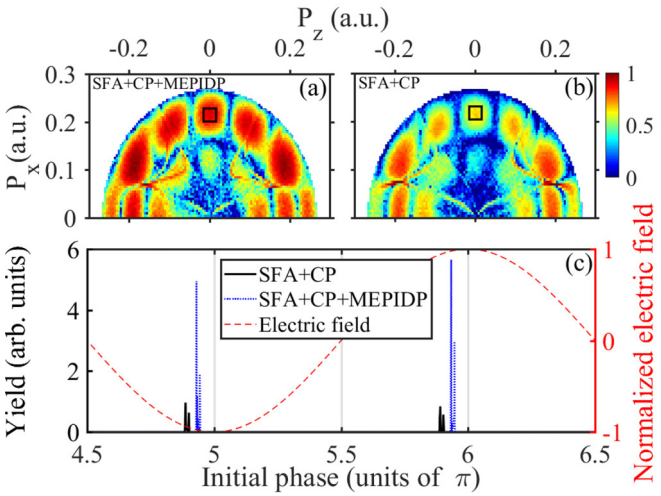

FIG. 4. (a) and (b) The momentum distributions ($P_x \geqslant 0$ a.u.) with (a) and without (b) considering the MEPIDP. (c) The initial ionization phase analysis of electron contributing to the final momentum indicated by a black rectangle in (a) and (b).

In addition, we also analyze the underlying physics of the probability enhancement induced by the MEPIDP. We choose a small region (black rectangle) in the photoelectron momentum spectrum with [Fig. 4(a)] and without [Fig. 4(b)] considering the MEPIDP and analyze the initial conditions of contributing electron trajectories which are shown in Fig. 4(c). The results indicate that for same final momentum, the electron would come from ionization time much closer to the laser peak where the ionization probability would be higher when the MEPIDP is considered, which explains the probability enhancement induced by the MEPIDP.

IV. CONCLUSION

In conclusion, we theoretically investigated the different contributions of the Coulomb potential, the MEPIDP, and the Stark shift to the PEMDs of Xe atoms driven by intense infrared laser fields. By comparing to the TDSE simulation, we found that the effect of MEPIDP was mainly manifested in the narrowing effect of the longitudinal momentum distributions and the enhancement of the LEIS yield, while the Stark shift

can induce the constructive interference among trajectories ionized from different half-cycle to the lower energy region, which plays an essential role of the formation of the LEIS in low-energy part of the PEMD. Our work reveals the importance of Stark shift which should be taken into account in the semiclassical methods for accurate description of the electron dynamics, especially the phase. As a result, our work would have great impact and applications for interpreting and reconstructing the structure and dynamical information with photoelectron holography where accurate description phase information is needed [60].

ACKNOWLEDGMENTS

The work was supported by the National Key Research and Development Program of China (Grants No. 2019YFA0307700 and No. 2016YFA0401100), NNSF of China (Grants No. 11774215, No. 12074240, and No. 91950101), Department of Education of Guangdong Province (Grant No. 2018KCXTD011), High Level University Projects of the Guangdong Province (Mathematics, Shantou University), and the Open Fund of the State Key Laboratory of High Field Laser Physics (SIOM).

[1] P. Agostini, F. Fabre, G. Mainfray, G. Petite, and N. K. Rahman, Phys. Rev. Lett. **42**, 1127 (1979).

[2] W. Becker, F. Grasbon, R. Kopold, D. B. Milošević, G. G. Paulus, and H. Walther, Adv. At Mol. Opt. Phys. **48**, 35 (2002).

[3] X. C. Gong, C. Lin, F. He, Q. Y. Song, K. Lin, Q. Y. Ji, W. B. Zhang, J. Y. Ma, P. F. Lu, Y. Q. Liu, H. P. Zeng, W. F. Yang, and J. Wu, Phys. Rev. Lett. **118**, 143203 (2017).

[4] X. H. Song, G. L. Shi, G. J. Zhang, J. W. Xu, C. Lin, J. Chen, and W. F. Yang, Phys. Rev. Lett. **121**, 103201 (2018).

[5] C. J. Zhang, W. F. Yang, X. H. Song, and Z. Z. Xu, Phys. Rev. A **79**, 043823 (2009).

[6] Z. J. Chen, Y. Y. Zheng, W. F. Yang, X. H. Song, J. L. Xu, L. F. Dimauro, O. Zatsarinny, K. Bartschat, T. Morishita, S. F. Zhao, and C. D. Lin, Phys. Rev. A, **92**, 063427 (2015).

[7] P. B. Corkum, Phys. Rev. Lett. **71**, 1994 (1993).

[8] L. V. Keldysh, Sov. Phys. JETP **20**, 1307 (1965).

[9] F. H. M. Faisal, J. Phys. B **6**, L89 (1973).

[10] T. M. Yan, S. V. Popruzhenko, and D. Bauer, Trajectory-based coulomb-corrected strong field approximation (Springer, Heidelberg, 2013).

[11] H. R. Reiss, Phys. Rev. A **22**, 1786 (1980).

[12] M. Lewenstein, P. Balcou, M. Yu. Ivanov, A. L. Huillier, and P. B. Corkum, Phys. Rev. A **49**, 2117 (1994).

[13] C. I. Blaga, F. Catoire, P. Colosimo, G. G. Paulus, H. G. Muller, P. Agostini, and L. F. DiMauro, Nat. Phys. **5**, 335 (2009).

[14] W. Quan, Z. Lin, M. Wu, H. Kang, H. Liu, X. Liu, J. Chen, J. Liu, X. T. He, S. G. Chen, H. Xiong, L. Guo, H. Xu, Y. Fu, Y. Cheng, and Z. Z. Xu, Phys. Rev. Lett. **103**, 093001 (2009).

[15] C. Y. Wu, Y. D. Yang, Y. Q. Liu, Q. H. Gong, M. Wu, X. Liu, X. L. Hao, W. D. Li, X. T. He, and J. Chen, Phys. Rev. Lett. **109**, 043001 (2012).

[16] C. Lemell, J. Burgdörfer, S. Gräfe, K. I. Dimitriou, D. G. Arbó, and X. M. Tong, Phys. Rev. A **87**, 013421 (2013).

[17] T. M. Yan, S. V. Popruzhenko, M. J. J. Vrakking, and D. Bauer, Phys. Rev. Lett. **105**, 253002 (2010).

[18] C. P. Liu and K. Z. Hatsagortsyan, Phys. Rev. Lett. **105**, 113003 (2010).

[19] A. Kästner, U. Saalmann, and J. M. Rost, Phys. Rev. Lett. **108**, 033201 (2012).

[20] L. Guo, S. S. Han, X. Liu, Y. Cheng, Z. Z. Xu, J. Fan, J. Chen, S. G. Chen, W. Becker, C. I. Blaga, A. D. DiChiara, E. Sistrunk, P. Agostini, and L. F. DiMauro, Phys. Rev. Lett. **110**, 013001 (2013).

[21] A. Rudenko, K. Zrost, C. D. Schröter, V. L. B. de Jesus, B. Feuerstein, R. Moshammer, and J. Ullrich, J. Phys. B **37**, L407 (2004).

[22] R. Gopal, K. Simeonidis, R. Moshammer, Th. Ergler, M. Dürr, M. Kurka, K. U. Kühnel, S. Tschuch, C. D. Schröter, D. Bauer, J. Ullrich, A. Rudenko, O. Herrwerth, Th. Uphues, M. Schultze, E. Goulielmakis, M. Uiberacker, M. Lezius, and M. F. Kling, Phys. Rev. Lett. **103**, 053001 (2009).

[23] H. Liu, Y. Liu, L. Fu, G. Xin, D. Ye, J. Liu, X. T. He, Y. Yang, X. Liu, Y. Deng, C. Wu, and Q. Gong, Phys. Rev. Lett. **109**, 093001 (2012).

[24] X. Y. Lai, S. G. Yu, Y. Y. Huang, L. Q. Hua, C. Gong, W. Quan, C. Figueira de Morisson Faria, and X. J. Liu, Phys. Rev. A **96**, 013414 (2017).

[25] D. G. Arbó, S. Yoshida, E. Persson, K. I. Dimitriou, and J. Burgdörfer, Phys. Rev. Lett. **96**, 143003 (2006).

[26] D. G. Arbó, K. I. Dimitriou, E. Persson, and J. Burgdörfer, Phys. Rev. A **78**, 013406 (2008).

[27] N. I. Shvetsov-Shilovski, M. Lein, and L. B. Madsen, Phys. Rev. A **98**, 023406 (2018).

[28] N. I. Shvetsov-Shilovski, M. Lein, L. B. Madsen, E. Räsänen, C. Lemell, J. Burgdörfer, D. G. Arbó, and K. T. Őkési, Phys. Rev. A **94**, 013415 (2016).

[29] A. N. Pfeiffer, C. Cirelli, M. Smolarski, D. Dimitrovski, M. Abusamha, L. B. Madsen, and U. Keller, Nat. Phys. **8**, 76 (2012).

[30] N. I. Shvetsov-Shilovski, D. Dimitrovski, and L. B. Madsen, Phys. Rev. A **85**, 023428 (2012).

[31] D. Dimitrovski, J. Maurer, H. Stapelfeldt, and L. B. Madsen, Phys. Rev. Lett. **113**, 103005 (2014).

[32] D. Dimitrovski and L. B. Madsen, Phys. Rev. A **91**, 033409 (2015).

[33] D. Dimitrovski, J. Maurer, H. Stapelfeldt, and L. B. Madsen, J. Phys. B **48**, 121001 (2015).

[34] H. P. Kang, S. P. Xu, Y. L. Wang, S. G. Yu, X. Y. Zhao, X. L. Hao, X. Y. Lai, T. Pfeifer, X. J. Liu, J. Chen, Y. Cheng, and Z. Z. Xu, J. Phys. B **51**, 105601 (2018).

[35] C. T. Le, V. H. Hoang, L. P. Tran, and V. H. Le, Phys. Rev. A **97**, 043405 (2018).

[36] D. Dimitrovski, C. P. J. Martiny, and L. B. Madsen, Phys. Rev. A **82**, 053404 (2010).

[37] T. Brabec, M. Côté, P. Boulanger, and L. Ramunno, Phys. Rev. Lett. **95**, 073001 (2005).

[38] Z. X. Zhao and T. Brabec, J. Mod. Opt. **54**, 981 (2007).

[39] Y. L. Wang, S. G. Yu, X. Y. Lai, X. J. Liu, and J. Chen, Phys. Rev. A **95**, 063406 (2017).
[40] X. H. Song, J. W. Xu, C. Lin, Z. H. Sheng, P. Liu, X. H. Yu, H. T. Zhang, W. F. Yang, S. L. Hu, J. Chen, S. P. Xu, Y. J. Chen, W. Quan, and X. J. Liu, Phys. Rev. A **95**, 033426 (2017).
[41] M. Li, J. W. Geng, H. Liu, Y. K. Deng, C. Y. Wu, L. Y. Peng, Q. H. Gong, and Y. Q. Liu, Phys. Rev. Lett. **112**, 113002 (2014).
[42] X. H. Song, C. Lin, Z. H. Sheng, P. Liu, Z. J. Chen, W. F. Yang, S. L. Hu, C. D. Lin, and J. Chen, Sci. Rep. **6**, 28392 (2016).
[43] C. Lin, H. T. Zhang, Z. H. Sheng, X. H. Yu, P. Liu, J. W. Xu, X. H. Song, S. L. Hu, J. Chen, and W. F. Yang, Acta Physica Sinica **65**, 223207 (2016).
[44] W. F. Yang, H. T. Zhang, C. Lin, J. W. Xu, Z. H. Sheng, X. H. Song, S. L. Hu, and J. Chen, Phys. Rev. A **94**, 043419 (2016).
[45] D. Dimitrovski, M. Abu-samha, L. B. Madsen, F. Filsinger, G. Meijer, J. Küpper, L. Holmegaard, L. Kalhøj, J. H. Nielsen, and H. Stapelfeldt, Phys. Rev. A **83**, 023405 (2011).
[46] T. Nakajima and G. Buica, Phys. Rev. A **74**, 023411 (2006).
[47] M. V. Ammosov, N. B. Delone, and V. P. Krainov, Sov. Phys. JETP **64**, 1191 (1986).
[48] N. B. Delone and V. P. Krainov, J. Opt. Soc. Am. B **8**, 1207 (1991).
[49] X. W. Liu, G. J. Zhang, J. Li, G. L. Shi, M. Y. Zhou, B. Q. Huang, Y. J. Tang, X. H. Song, and W. F Yang, Phys. Rev. Lett. **124**, 113202 (2020).
[50] S. D. Yang, X. H. Song, X. W. Liu, H. D. Zhang, G. L. Shi, X. H. Yu, Y. J. Tang, J. Chen, and W. F. Yang, Las. Phys. Lett. **17**, 095301 (2020).
[51] V. P. Shevelko and A. V. Vinogradov, Phys. Scr. **19**, 275 (1979).
[52] W. F. Yang, X. H. Song, Z. N. Zeng, R. X. Li, and Z. Z. Xu, Opt. Express **18**, 2558 (2010).
[53] W. F. Yang, X. H. Song, and Z. J. Chen, Opt. Express **20**, 12067 (2012).
[54] W. F. Yang, Z. H. Sheng, X. P. Feng, M. L. Wu, Z. J. Chen, and X. H. Song, Opt. Express **22**, 2519 (2014).
[55] I. W. Sudiarta and D. J. W. Geldart, J. Phys. A: Math. Theor. **40**, 1885 (2007).
[56] D. B. Milošević, W. Becker, M. Okunishi, G Prümper, K. Shimada, and K. Ueda, J. Phys. B **43**, 015401 (2010).
[57] F. Lindner, M. G. Schätzel, H. Walther, A. Baltuška, E. Goulielmakis, F. Krausz, D. B. Milošević, D. Bauer, W. Becker, and G. G. Paulus, Phys. Rev. Lett. **95**, 040401 (2005).
[58] D. G. Arbó, E. Persson, and J. Burgdörfer, Phys. Rev. A **74**, 063407 (2006).
[59] D. G. Arbó, K. L. Ishikawa, K. Schiessl, E. Persson, and J. Burgdörfer, Phys. Rev. A **82**, 043426 (2010).
[60] C. F. D. M. Faria and A. S. Maxwell, Rep. Prog. Phys. **83**, 034401 (2020).